University of Tehran

School of Mechanical Engineering

Adaptive Control

Final Project

Professor:

Dr. Moosa Ayati

Author:

Masoud Pourghavam

June, 2023

Table of Contents

List of Figures

List of Tables

Abstract

Real-time hybrid simulation (RTHS) is an innovative technique used to examine complex and large structural systems. It involves the use of controllers to compensate for the dynamics of transfer systems that mimic the interactions between physical and numerical components. The success of RTHS testing depends greatly on the control strategy's effectiveness in ensuring stability and accuracy. This study introduces a reliable sliding mode controller (SMC) as a control strategy for transfer systems in RTHS. The paper presents a step-by-step process for designing the SMC control strategy and utilizes a benchmark problem on RTHS control to demonstrate and validate its effectiveness. Virtual RTHS results indicate that the SMC strategy considerably enhances the performance and robustness of RTHS testing.

Keywords:

Sliding mode control, Phase-lead compensator, Benchmark, Hybrid simulation, Kalman estimator

1. Introduction

Full-scale dynamic tests of structures, such as buildings and bridges, can be costly, time-consuming, and limited by the equipment available. Real-time hybrid simulation (RTHS) has emerged as an attractive alternative over the past two decades. RTHS divides the structure into numerical and physical substructures, using actuators or loading devices to enforce interface conditions between them [1–8]. The performance of the RTHS is highly dependent on the controller driving the transfer system [9,10]. Designing a high-performance controller in RTHS presents challenges, including addressing time delays, time lags, modeling uncertainties, measurement noise, and external disturbances [11–13]. Time delays and lags in the feedback loop can introduce negative damping and potentially lead to system instability [14]. Various compensation techniques have been developed to address these challenges, such as phase-lead compensation, inverse-based feed-forward compensation, and adaptive compensation [7,15–21]. Additionally, the controller in RTHS must be robust enough to handle uncertainties, noise, and disturbances, ensuring accurate tracking and system stability. Robust control design has been a focus in developing high-quality RTHS methods [10,22–24].

Benchmark problems serve as valuable tools for comparing different techniques on a common problem with well-defined metrics. The civil engineering community has established benchmark problems in structural control since the 1990s, fostering advancements in hazard mitigation [25–30]. Recently, an RTHS benchmark problem was introduced to drive advances in control strategies for compensating for the dynamics of the transfer system during RTHS experiments on a three-story steel frame [31]. Researchers are tasked with replacing the demo controller in the benchmark simulation with their own designs and evaluating their performance and robustness through virtual RTHS. Several researchers have proposed their controllers or control systems for this problem, such as robust H1 controllers, control systems with feedforward compensators and feedback regulators, back-stepping controllers with state estimation and time lag compensation, controllers treating time lag as negative damping and model-based control systems with adaptation laws [32–35].

However, previous studies on this benchmark problem have focused on designing model-based controllers or control systems based on a fifth-order control plant. Noise amplification in the higher-order states must be carefully addressed to maintain control performance. In this paper, a robust model-based sliding mode control system is developed for the RTHS benchmark

problem using a reduced second-order control plant. The control problem is defined, including associated uncertainties. Detailed formulations of the sliding mode controller, Kalman estimator, and phase-lead compensator are presented. Numerical simulations are conducted to evaluate the performance and robustness of the controller design under different partitioning cases and ground motions. Building on previous studies on sliding mode controllers in RTHS [10,36], this benchmark problem considers increasingly challenging partitioning cases to demonstrate the sliding mode approach's high performance in the presence of significant uncertainty. The paper aims to illustrate an important advantage of the sliding mode control system, namely, the ability to replace a higher-order control plant with uncertainties with a relatively lower-order control plant without compromising performance and robustness.

2. Control plant of benchmark problem

The benchmark problem centers around a reference structure consisting of three degrees of freedom (DOF). During the partitioning process in real-time hybrid simulation (RTHS), a specific portion of the reference model's first floor is designated as the physical substructure, illustrated in Figure 1. The rest of the reference structure is treated as a numerical subsystem. For detailed and extensive information regarding the benchmark problem, it is advised to consult the problem definition paper [31]. The primary focus of this section is directed toward the control plant involved in the benchmark problem.

2.1 Original model of the input

Fig. 2 shows the block diagram of the control plant including the dynamics of the servo-hydraulic actuator and physical substructure. In Fig. 2, y_{Gc} is the command signal input to the transfer system (the servo-controlled hydraulic actuator); f_e is the actuator force, which becomes the feedback to the numerical substructure; x_m is the displacement of the physical substructure, which is the feedback to the controller; s is the Laplace variable; $a_1\beta_0, \beta_1$and β_2 are parameters related to the servo-valve dynamics, a_2, and a_3 are parameters associated with the actuator dynamics [31,37,38]; m_e, c_e and k_e are the mass, damping coefficient, and stiffness of the physical substructure. Table 1 lists values of these parameters [31] with standard deviations on a_3, β_1, β_2, and k_e to consider parametric uncertainties. According to Fig. 2, the transfer function from y_{Gc} to x_m is

$$G_p(s) = \frac{B_0}{A_5 s^5 + A_4 s^4 + A_3 s^3 + A_2 s^2 + A_1 s^1 + A_0} \tag{1}$$

where,

$$\begin{aligned}
B_0 &= a_1\beta_0 \\
A_0 &= k_e a_3\beta_2 + a_1\beta_0 \\
A_1 &= k_e a_3\beta_1 + (k_e + c_e a_3 + a_2)\beta_2 \\
A_2 &= k_e a_3 + (k_e + c_e a_3 + a_2)\beta_1 + (c_e + m_e a_3)\beta_2 \\
A_3 &= k_e + c_e a_3 + a_2 + (c_e + m_e a_3)\beta_1 + m_e\beta_2 \\
A_4 &= c_e + m_e a_3 + m_e\beta_1 \\
A_5 &= m_e
\end{aligned} \tag{2}$$

Eq. (1) represents the original model of the control plant, which is a physics-based fifth-order linear model.

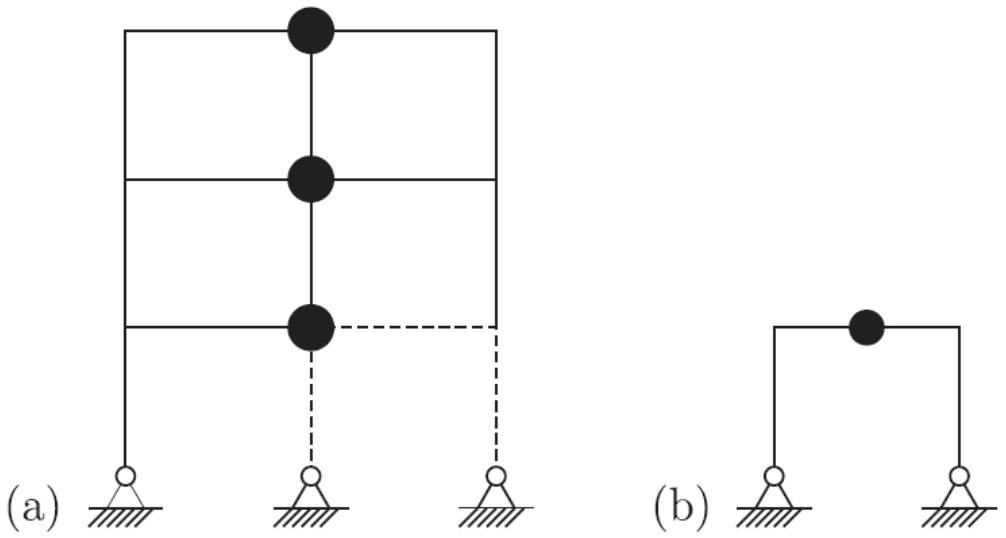

Fig 1. Sketch of the RTHS partitioning: (a) reference structure; (b) physical substructure

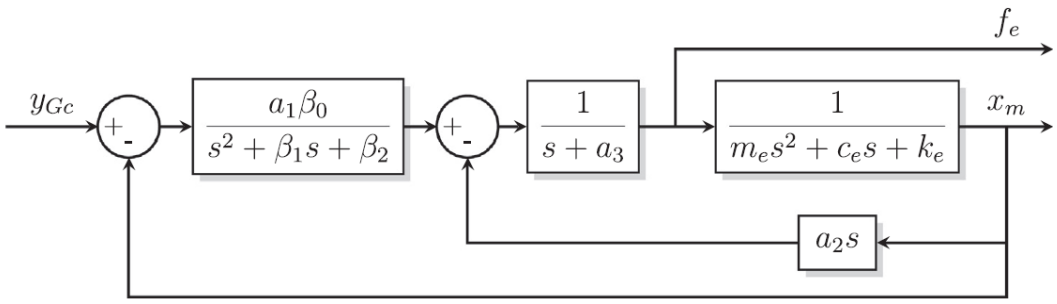

Fig 2. Block diagram of the control plant

Table 1. Parametric values and uncertainties associated with the original model of the control plant

Parameter	Nominal value	Standard deviation	Units
$a_1\beta_0$	2.13×10^{13}	-	kg/s^5
a_2	4.23×10^6	-	kg/s^2
a_3	3.3	1.3	s^{-1}
β_1	425	3.3	s^{-1}
β_2	1×10^5	3.31×10^3	s^{-2}
m_e	29.1	-	kg
c_e	114.6	-	kg/s
k_e	1.19×10^6	5×10^4	kg/s^2

2.2 Reduced-order model of the control plant

The dynamics of Eq. (1) can be reduced into

$$G_{pr}(s) = \frac{a}{s^2 + bs + c} \times \left(\frac{1 + ds}{1 + es} \right) \tag{3}$$

where *a*, *b*, *c*, *d* and *e* are positive parameters that need to be determined. By defining the adjusted command *u* as

$$u = \frac{a(1 + ds)}{1 + es} y_{Gc} \tag{4}$$

the transfer function from *u* to x_m is given by

$$G_r(s) = \frac{1}{s^2 + bs + c} \tag{5}$$

To differentiate, y_{Gc} is referred to as actual command hereafter. Eq. (5) is defined as the adjusted control plant. Uncertainties of the original model Eq. (1) could be reflected in the uncertainty of parameters *b* and *c* in the reduced-order model Eq. (3). The identified reduced-order model parameters and their respective uncertainties are listed in Table 2. The frequency responses of both original and reduced-order models up to $30Hz$ are shown in Fig. 3, where the model uncertainties of the original model Eq. (1) are encompassed by the results of the reduced-order model Eq. (3). In the next section we present the sliding mode control design for the adjusted control plant Eq. (5). The sliding mode controller (SMC) generates the adjusted command *u*. Once *u* is obtained, the actual command y_{Gc} sent to the fifth-order control plant (Fig. 2) is calculated based on Eq. (4).

Table 2. Parametric values and uncertainties associated with the reduced-model of the control plant

Parameter	Nominal value	Uncertainty	Units
a	53354	--	s^{-2}
b	221.64	[141.85,301.43]	s^{-1}
c	54290	[48861,59719]	s^{-2}
d	1.06×10^{-4}	--	s
e	2.11×10^{-2}	--	s

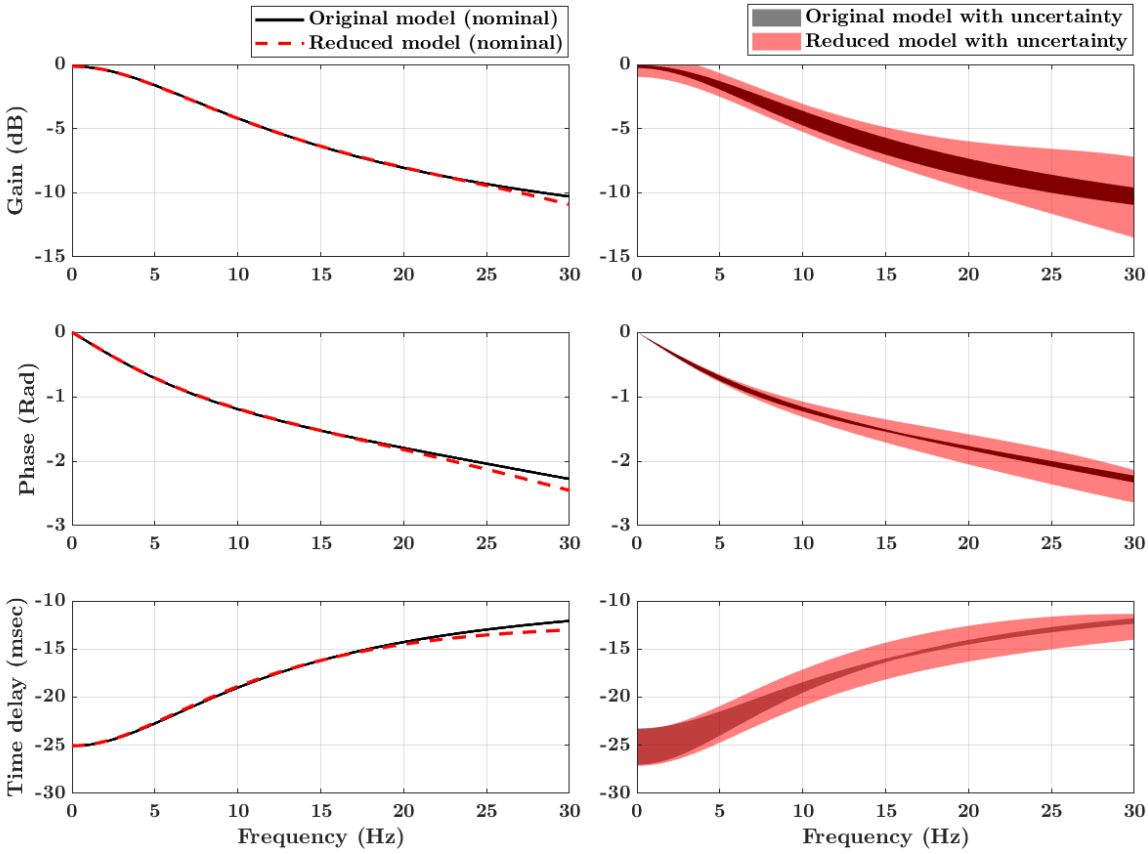

Fig 3. Frequency responses of original and reduced-order models of the control plant (left: nominal models; right: models with uncertainties)

3. Sliding mode control design

Sliding mode control is a robust control method aimed at dealing with model uncertainty in both linear and nonlinear systems [10,39]. For an nth-order system, the control law is formed based on a compact scalar error combining errors of (n-1) variables (normally the states of the system). It converts a tracking problem of multiple variables into a stabilization problem of the compact scalar error. High performance and robustness can be achieved in the presence of parametric inaccuracies. Thus, sliding mode control is chosen in this paper. In this section, the sliding mode control system containing a Kalman estimator, an SMC, and a phase-lead compensator is presented.

3.1 Kalman estimator

SMC requires full-state feedback. However, the control plant in the benchmark problem only provides displacement measurement with additional sensor noise. Thus, a Kalman estimator [40] is adopted to estimate the state of the plant. The nominal model of the adjusted control plant Eq. (5) is used to deploy the Kalman estimator. According to the definition of the benchmark problem, the measurement noise of x_m is modeled as a Gaussian white process with the power spectral density (PSD) of $2.56 \times 10^{-10} m^2$. Assuming there is no process noise, the state-space representation for the adjusted control plant is

$$\begin{aligned} \dot{X} &= Ax + Bu \\ X_m &= Cx + \nu \end{aligned} \tag{6}$$

Where $x = [x_m, \dot{x}_m]^T$, v is the white noise with the variance of $2.56 \times 10^{-10}\, m^2$,

$$\begin{aligned} A &= \begin{bmatrix} 0 & 1 \\ -\bar{c} & -\bar{b} \end{bmatrix} \\ B &= \begin{bmatrix} 0 \\ 1 \end{bmatrix} \\ C &= [10] \end{aligned} \tag{7}$$

$\bar{b} = 221.64 s^{-1}$ and $\bar{C} = 54290 s^{-2}$

The MATLAB [41] Simulink block Kalman Filter is used here, which computes the optimal gain vector **L** to obtain the estimated state $\hat{x}$ that eliminates noise effects online according to the following state equation:

$$\dot{\hat{x}} = A\hat{x} + Bu + L(x_m - C\hat{x})$$
$$\text{where } \hat{x} = \left[\hat{x}_m, \dot{\hat{x}}_m\right]^T$$

3.2 Sliding mode controller

The time domain representation of Eq. (5) using the estimated variables is

$$\ddot{\hat{x}}_m = f(\hat{x}_m) + u \tag{9}$$

where the function $f(.)$ is defined as

$$f(\Delta) = -b\dot{\Delta} - c\Delta \tag{10}$$

The nominal representation of $f(.)$ is

$$\bar{f}(\Delta) = -\bar{b}\dot{\Delta} - \bar{c}\Delta \tag{11}$$

The modeling error on $f(.)$ is bounded by $f(.)$, defined as follows

$$\left|\bar{f}(\Delta) - f(\Delta)\right| \le F(\Delta) = \tilde{b}\left|\dot{\Delta}\right| + \tilde{c}\left|\Delta\right| \tag{12}$$

where according to Table 2,

$$\tilde{b} = \frac{301.43 - 141.85}{2} = 79.79 s^{-1}$$
$$\tilde{c} = \frac{59719 - 48861}{2} = 5429 s^{-2} \tag{13}$$

Let

$$e = \hat{x}_m - x_d \tag{14}$$

be the displacement tracking error, where x_d is the designated displacement calculated from the numerical substructure. The compact error is defined as

$$E = \dot{e} + \lambda e \tag{15}$$

where λ is a strictly positive constant. The goal of the controller is to ensure the convergence of the compact error to zero, which can be achieved using Barbalet's lemma [39]. Here we choose the Lyapunov function

$$V = \frac{E^2}{2} \tag{16}$$

That satisfies

$$\dot{V} = E\dot{E} \leq -\eta|E| \tag{17}$$

where λ is a strictly positive constant. Eq. (17) is referred to as the sliding condition. Because

$$\dot{E} = f(\hat{x}_m) + u - \ddot{x}_d + \lambda\dot{e} \tag{18}$$

the nominal command that would achieve $\dot{E} = 0$ is

$$\bar{u} = -\bar{f}(\hat{x}_m) + \ddot{x}_d - \lambda\dot{e} \tag{19}$$

In order to satisfy the sliding condition Eq. (17) with parametric uncertainties, a discontinuous term across the sliding surface $E = 0$ is added to u. It can be proven that the control law

$$u' = \bar{u} - k\,\mathrm{sgn}(E) \tag{20}$$

With

$$k = F(\hat{x}_m) + \eta \tag{21}$$

satisfies the sliding condition. The second term $ksgn(E)$ in Eqs. (20) is called the correction term and $sgn(.)$ is the sign function:

$$\mathrm{sgn}(E) = \begin{cases} 1 & E > 0 \\ 0 & E = 0 \\ -1 & E < 0 \end{cases} \tag{22}$$

One drawback of the control law shown in Eq. (20) is that the $sgn(E)$ function might cause chattering (oscillations across the sliding surface) in the control command. To eliminate chattering so that the controller can perform adequately, $sgn(E)$ in Eq. (20) is replaced by the following saturation function

$$sat(E/\Phi)=\begin{cases} E/\Phi & |E/\Phi|\le 1 \\ \mathrm{sgn}(E) & |E/\Phi|>1 \end{cases} \tag{23}$$

Thus, the control discontinuity can be smoothed by creating a boundary layer Φ neighboring the switching surface $E = 0$, as shown in Fig. 4. The thickness of the boundary Φ can be tuned in real-time so that $\dot{E}$ always represents a first-order filter of E with bandwidth λ. As a result, the final control law can be deduced as

$$u=\bar{u}-\bar{k}sat(E/\Phi) \tag{24}$$

where,

$$\bar{k}=k-\dot{\Phi} \tag{25}$$

And Φ satisfies

$$\dot{\Phi}=F(x_d)+\eta-\lambda\Phi \tag{26}$$

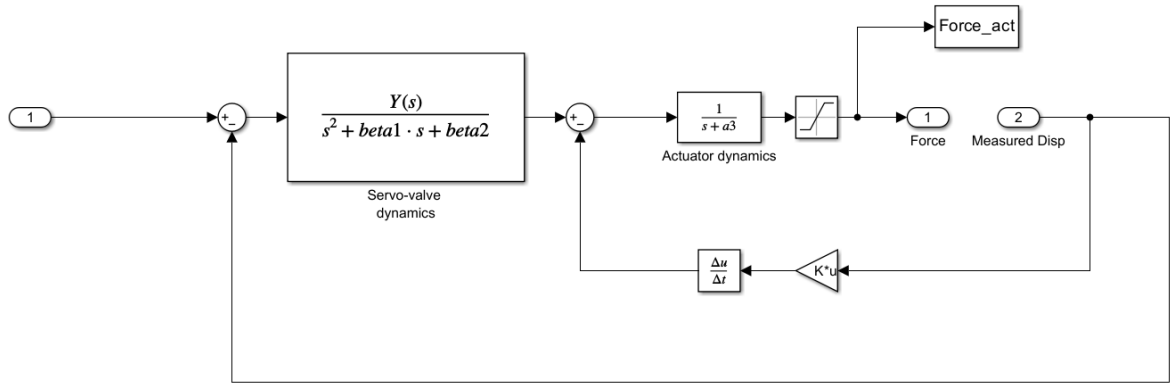

Fig 4. Sliding mode controller model

3.3 Phase-lead compensator

Time delays in RTHS generally occur due to a combination of communication delay, computation delay, and the delay from analog-to-digital (A/D) conversion. Meanwhile, the time lag is caused by the inherent dynamics of the transfer system [42,43]. As long as the parameters of SMC (λ and η) are well-tuned, the time lag can be minimized and even ignored [10,36]. Virtual real-time execution of the benchmark problem is conducted at a fixed time step $\tau = 2.4414 \times 10^{-4}$ (sampling frequency is 4096 Hz). As a complement to this approach, we consider the communication and computation delays by combining them to form a single pure time delay s. Thus, the phase-lead compensator is designed as

$$e^{\tau s} = \frac{e^{2\tau s}}{e^{\tau s}} \approx \frac{1+2\tau s}{1+\tau s} = G_{pl}(s) \tag{27}$$

With these choices, the overall RTHS block diagram including the detailed setup of the whole control system is shown in Fig. 5, where $\ddot{x}_g$ is the ground motion.

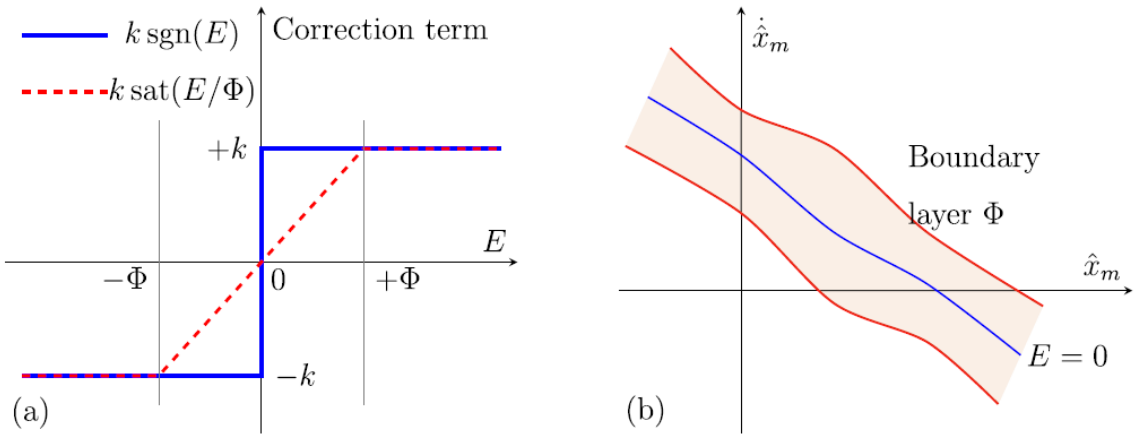

Fig 5. (a) Correction term of the control command with and without boundary layer: (b) Sketch of the sliding surface and time-varying boundary layer

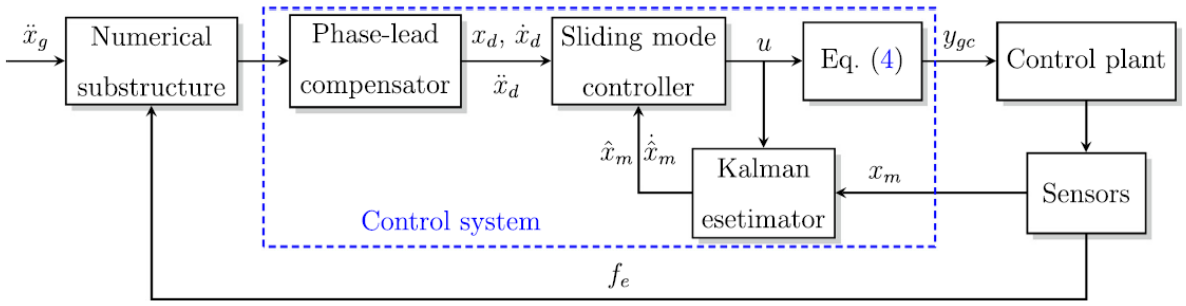

Fig 6. RTHS block diagram

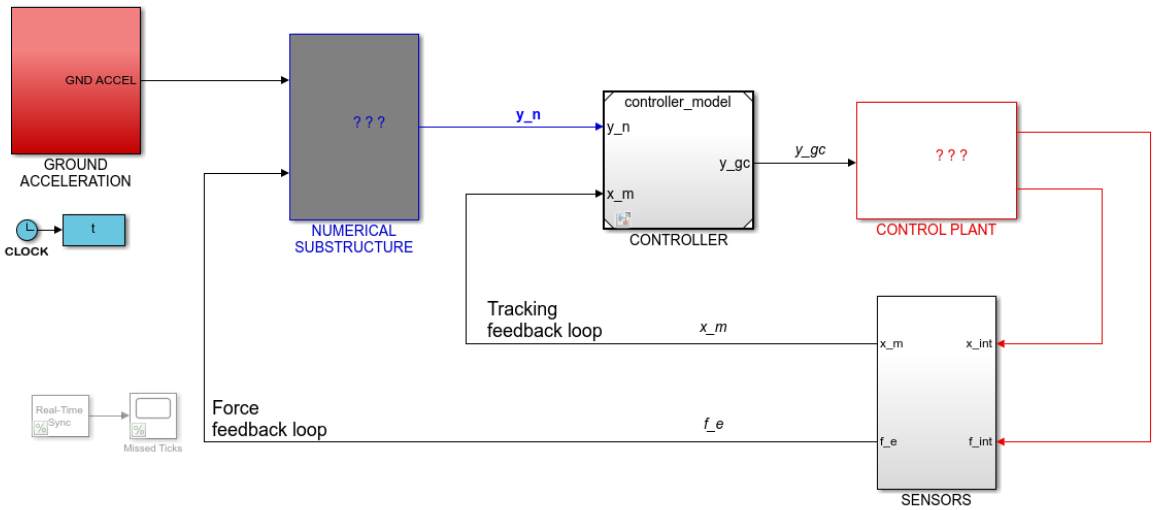

Fig 7. Phase-lead compensator model

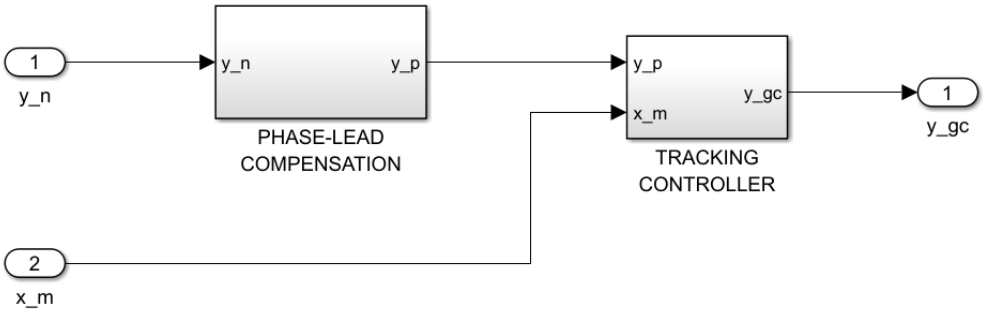

Fig 8. Controller model

4. Simulation results

The ground acceleration data consists of three separate ground motion records: El Centro 1940, Kobe 2005, and Morgan Hill 1984, plus a linear sinusoidal sweep signal ($0.1\sim40Hz$, time duration: $90\ s$). Four RTHS partitioning cases are selected in the benchmark problem, see Table 3. The predictive stability indicator (PSI) represents the sensitivity of the partitioning choice [13,44]. In the benchmark problem, the PSIs of the partitioning cases lie in different sensitivity regions [31]. The controller is not especially sensitive to the parameter g, and it is chosen as $\eta = 0.1$. According to Fig. 3, the reduced order model is valid up to $30Hz$. Thus, we set $\lambda = 30Hz = 188s^{-1}$. For demonstration purposes, only the results of the El Centro earthquake are shown in this section. Fig. 6 shows the adjusted command u for Case 4 using the nominal control plant. The adjusted command is smoothed with the adoption of the boundary layer. Although from Fig. 6, the chattering present in the unsmoothed adjusted command (no boundary layer used) seems to be acceptable, it would actually cause an extremely high-level of chattering in the actual command, as shown in Fig. 7. Thus, without the adoption of a boundary layer, high-frequency unmodeled dynamics of the control plant will be generated, which decreases the controller performance. Fig. 8 plots the compact error trajectory as well as the boundary layer. The compact error is kept at a very low level with a maximal absolute compact error of $6.21 \times 10^{-16}\ m/s$, indicating good tracking performance of the controller. However, without using the boundary layer, the maximal absolute compact error is $3.1 \times 10^{-3}\ m/s$ (increased by a factor of 5.4×10^{13}).

Table 3. RTHS partitioning cases of the benchmark problem

Partitioning Case (#)	Reference floor (kg)	Reference modal damping (%)
Case 1	1000	5
Case 2	1100	4
Case 3	1300	3
Case 4	1000	3

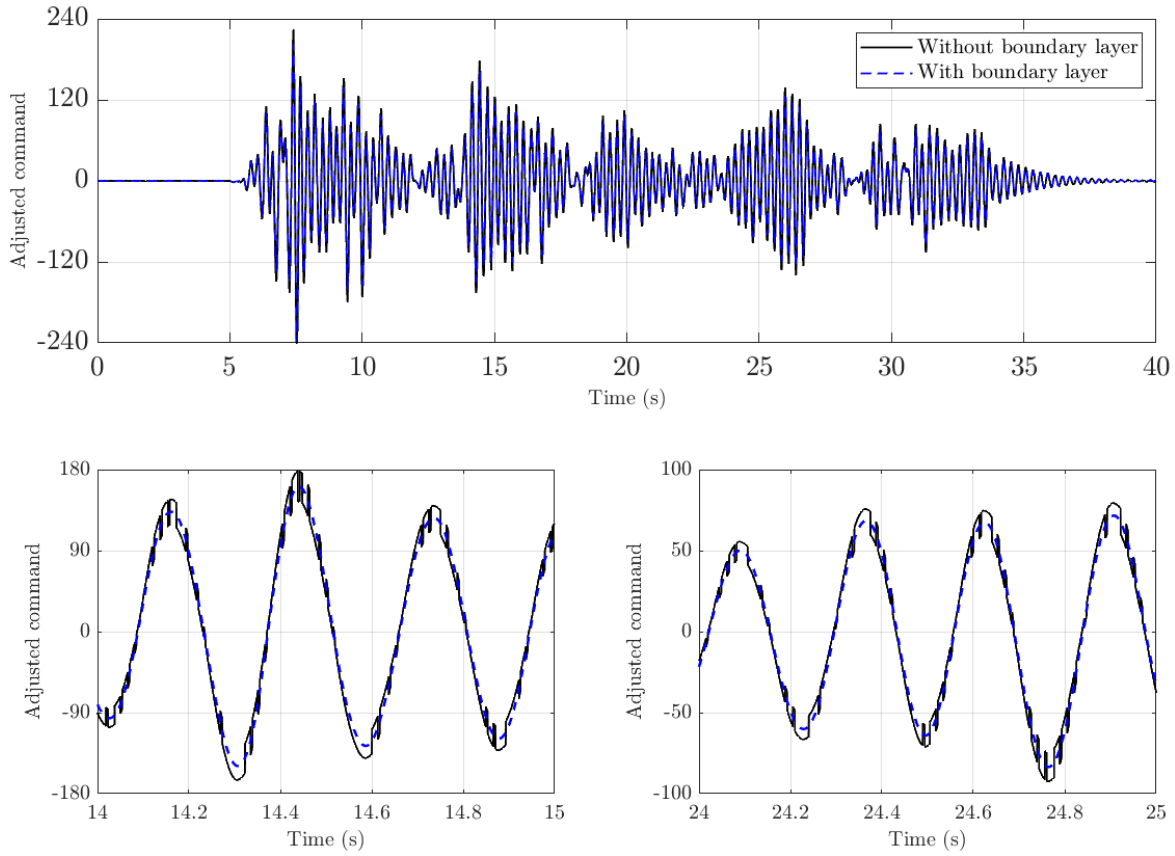

Fig 9. Adjusted command: EL Centro earthquake, case 4, nominal control plant

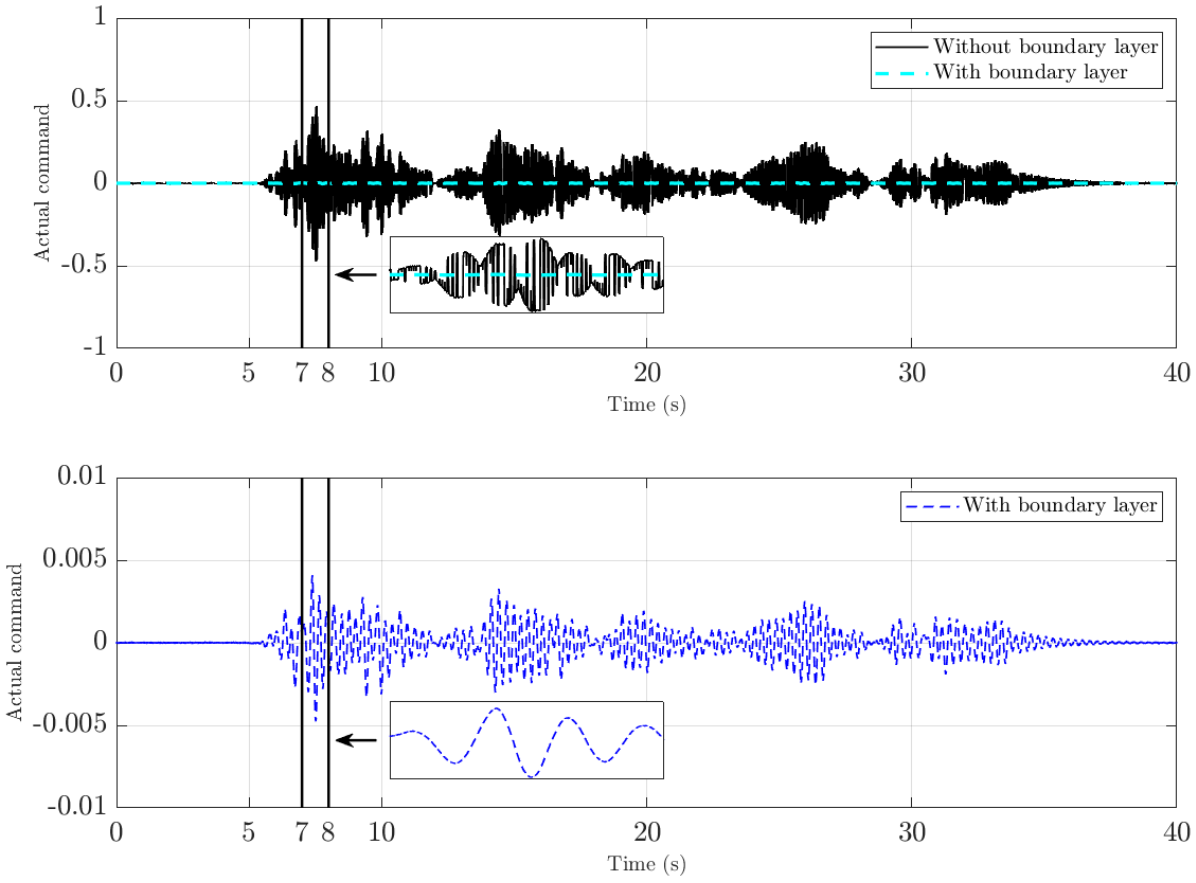

Fig 10. Actual command: El Centro earthquake, case 4, nominal control plant

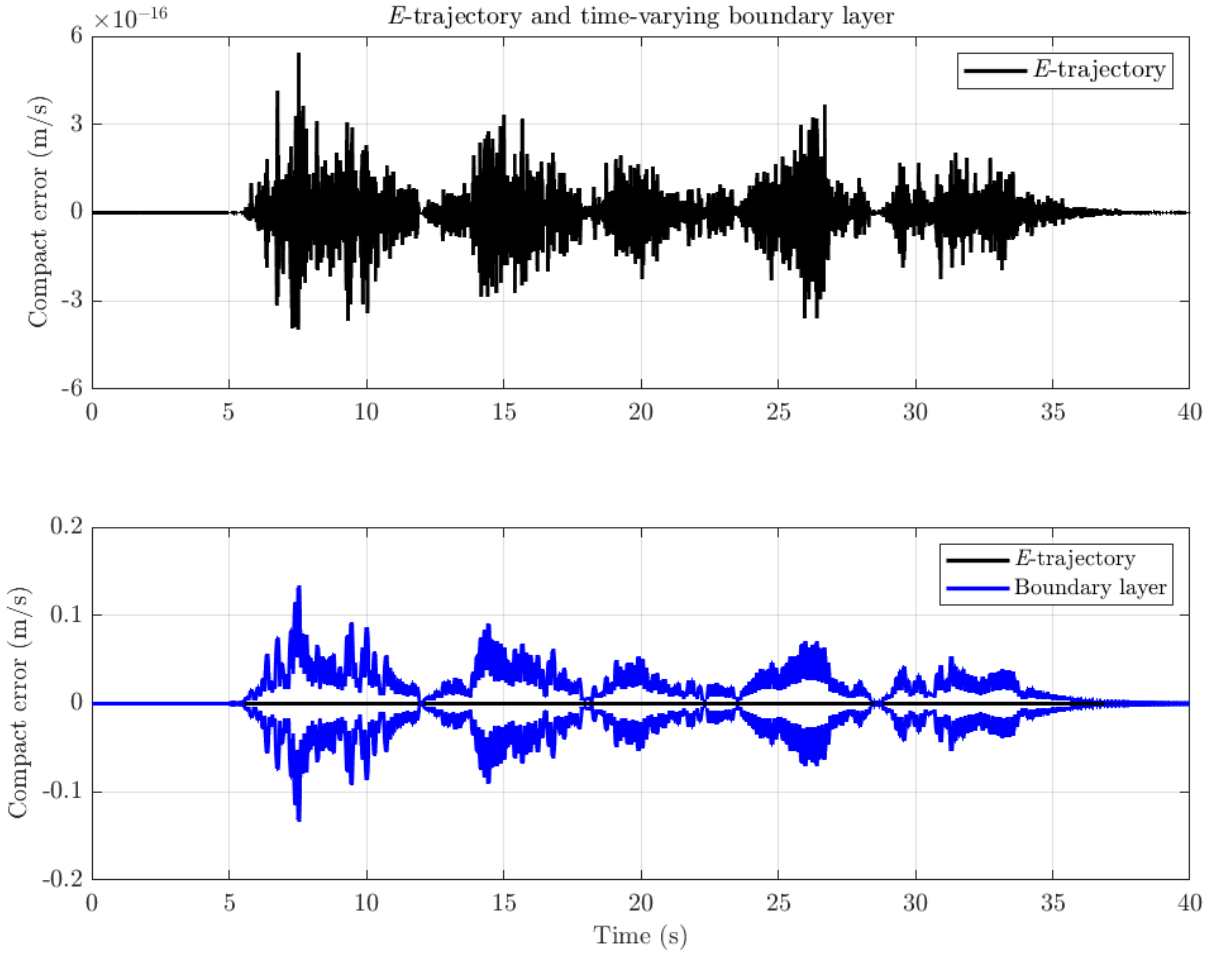

Fig 11. Compact error trajectory and time-varying boundary layer: El Centro earthquake, Case 4, nominal control plant

Comparisons of the floor displacements are shown in Fig. 9, where PI P refers to the benchmark demo controller: a proportional-integral controller with a phase-lead compensator. From the results, using the SMC significantly enhances the performance of the virtual RTHS compared to using PI-P. To quantitatively evaluate the performance of controllers through virtual RTHS, nine evaluation criteria from J_1 to J_9 are to be calculated. J_1 is the tracking time delay, J_2 and J_3 are the normalized root mean square (NRMS) error and the normalized peak error for the controller displacement tracking. The remaining evaluation criteria compare the responses in the virtual RTHS and the reference model to evaluate the global performance of the virtual RTHS. More detailed descriptions of these criteria can be found in [31]. Tables 4 and 5 lists the evaluation criteria under the El Centro earthquake for SMC and PI-P, respectively. Due to space limitations, only the results for PI-P using the nominal control plant are listed here. Five perturbed control plants are considered for SMC in each partitioning case. The largest value

associated with each partitioning case is emboldened in Table 5. As presented in Table 5, the time delay J_1 remains at zero in all cases. J_2 to J_9 of SMC are kept at a low level (mostly less than 4%) with maximal values of 0.54%, 0.58%, 6.17%, 4.17%, 6.24%, 6.24%, 4.30%, and 4.32%, which are much less (decreased by over 80%) than those of PI-P. Evaluation criteria under Kobe, Morgan earthquakes, and the chirp excitation (see Appendix A) have the same level compared with those under the El Centro earthquake. It can be concluded that the virtual RTHS using SMC exhibits good tracking performance and robustness.

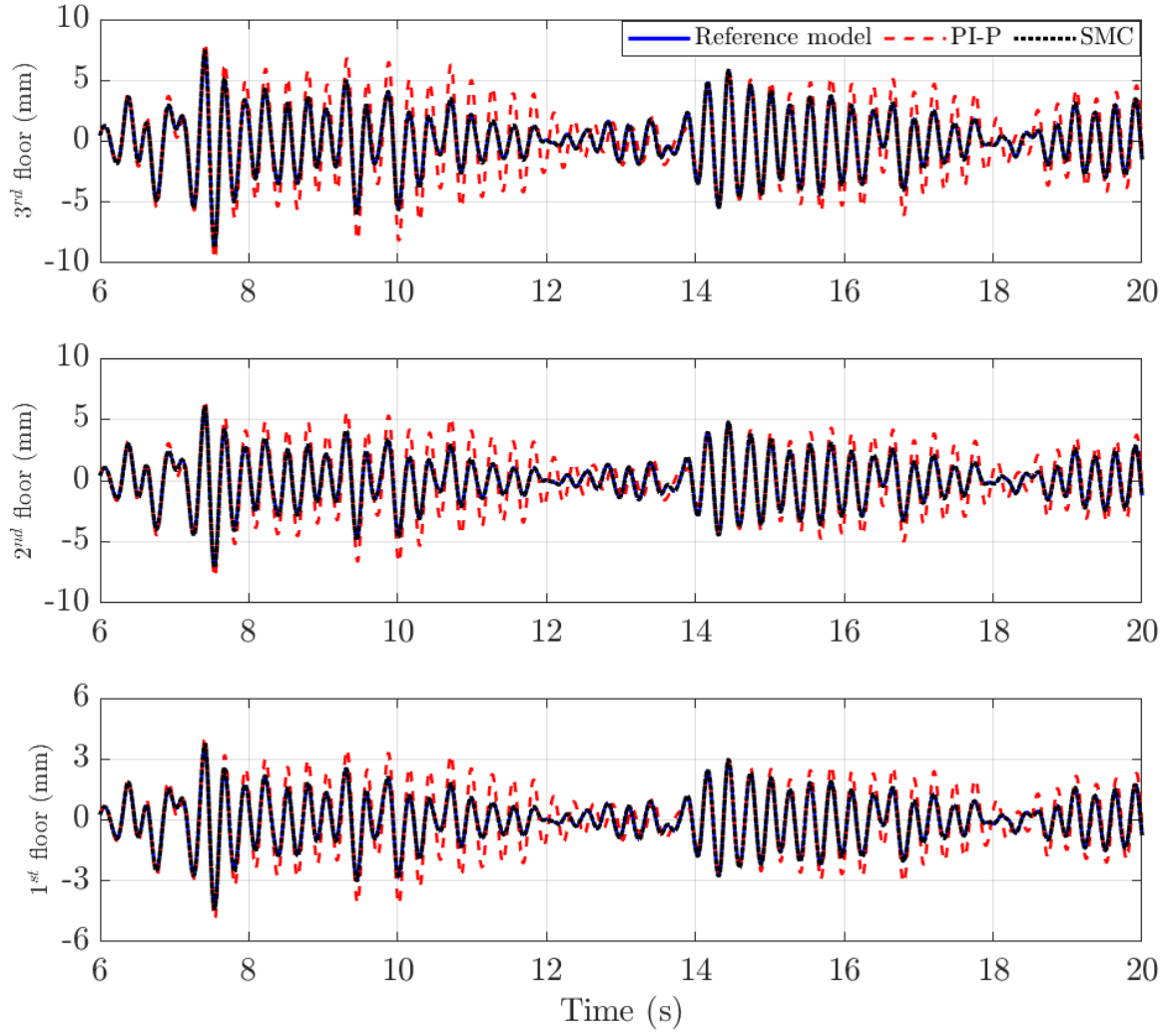

Fig 12. Floor displacement in the reference model and virtual RTHS: El Centro earthquake, case 4, nominal control plant

Table 4. Evaluation criteria under El Centro earthquake, controller: PI-P

Partitioning Case (#)	J_1 (msec)	J_2 (%)	J_3 (%)	J_4 (%)	J_5 (%)	J_6 (%)	J_7 (%)	J_8 (%)	J_9 (%)
Case 1	4.6	10.38	11.54	36.08	19.01	32.26	32.38	14.85	14.78
Case 2	4.6	9.81	11.08	33.06	17.05	30.45	30.54	15.26	15.21
Case 3	4.6	9.04	10.18	49.85	36.67	49.79	49.80	35.53	35.59
Case 4	4.6	10.47	11.31	72.61	35.19	68.55	68.71	33.45	33.32

Table 5. Evaluation criteria under El Centro earthquake, controller: SMC

Partitioning Case (#)		J_1 (msec)	J_2 (%)	J_3 (%)	J_4 (%)	J_5 (%)	J_6 (%)	J_7 (%)	J_8 (%)	J_9 (%)
Case 1	Nominal	0	0.53	**0.58**	1.00	0.64	0.88	0.89	0.47	0.47
	Perturbed 1	0	0.53	0.57	3.71	1.98	3.98	3.99	2.09	2.10
	Perturbed 2	0	0.53	0.58	2.68	1.49	2.48	2.49	1.34	1.34
	Perturbed 3	0	0.53	0.58	2.34	1.31	2.00	2.01	1.07	1.07
	Perturbed 4	0	0.53	0.58	2.54	1.38	2.44	2.45	1.29	1.29
	Perturbed 5	0	0.53	0.58	1.17	0.72	1.48	1.49	0.79	0.79
Case 2	Nominal	0	0.50	0.56	0.97	0.60	0.83	0.83	0.45	0.45
	Perturbed 1	0	0.50	0.56	2.49	1.40	2.17	2.18	1.20	1.20
	Perturbed 2	0	0.50	0.56	1.75	0.99	1.95	1.96	1.08	1.08
	Perturbed 3	0	0.50	0.56	0.47	0.47	0.55	0.55	0.31	0.31
	Perturbed 4	0	0.50	0.56	2.86	1.60	2.63	2.63	1.45	1.45
	Perturbed 5	0	0.50	0.55	3.66	1.95	3.63	3.64	1.96	1.96
Case 3	Nominal	0	0.47	0.52	1.36	0.91	1.20	1.20	0.83	0.83
	Perturbed 1	0	0.47	0.52	3.36	2.28	3.18	3.17	2.19	2.20
	Perturbed 2	0	0.47	0.52	2.48	1.73	2.44	2.43	1.68	1.68
	Perturbed 3	0	0.47	0.52	4.99	3.37	4.88	4.88	3.36	3.37
	Perturbed 4	0	0.47	0.52	5.03	3.46	4.79	4.79	3.30	3.31
	Perturbed 5	0	0.47	0.52	**6.17**	**4.17**	**6.24**	**6.24**	**4.30**	**4.32**
Case 4	Nominal	0	**0.54**	0.57	1.51	0.80	1.48	1.49	0.74	0.74
	Perturbed 1	0	0.54	0.57	4.08	2.10	3.69	3.70	1.87	1.86
	Perturbed 2	0	0.54	0.57	2.01	1.08	2.29	2.29	1.15	1.15
	Perturbed 3	0	0.54	0.57	2.60	1.36	2.42	2.42	1.22	1.22
	Perturbed 4	0	0.54	0.57	3.36	1.70	3.05	3.06	1.54	1.53
	Perturbed 5	0	0.54	0.57	4.49	2.32	4.49	4.50	2.26	2.25

5. Conclusion

In this paper, a model-based sliding mode control strategy is presented, incorporating a Kalman estimator and a phase-lead compensator. The study focuses on the design and evaluation of this control strategy using the RTHS control benchmark problem. The main objective is to demonstrate that a lower-order control plant with uncertainties can effectively replace a higher-order control plant, without compromising performance and robustness. The original fifth-order control problem in the benchmark is simplified to a second-order control problem with parametric uncertainties, and the sliding mode control system is designed based on this reduced control plant.

To assess the performance of the sliding mode control system, simulations are conducted considering different ground motions and partitioning configurations. The evaluation is carried out using the nine criteria specified in the benchmark problem. The results indicate the following:

- The sliding mode control system exhibits significantly improved robustness and accuracy compared to the demo controller provided in the benchmark problem.
- The proposed control strategy is expected to be highly effective for complex control plants.

Overall, this study demonstrates the effectiveness of the sliding mode control system in the RTHS context, showcasing its ability to handle uncertainties and achieve desirable control performance with a reduced-order control plant.

References

[1] T. Horiuchi, M. Inoue, T. Konno, Y. Namita, Real-time hybrid experimental system with actuator delay compensation and its application to a piping system with energy absorber, Earthquake Engineering & Structural Dynamics 28 (10) (1999) 1121–1141.
[2] R. Christenson, Y.Z. Lin, A. Emmons, B. Bass, Large-scale experimental verification of semiactive control through real-time hybrid simulation, Journal of Structural Engineering 134 (4) (2008) 522–534.
[3] X. Gao, N.E. Castaneda, S.J. Dyke, S. Xi, C.D. Gill, C. Lu, Y. Ohtori, Experimental validation of a scaled instrument for real-time hybrid testing, in: Proceedings of the 2011 American Control Conference, IEEE, 2011, pp. 3301–3306.
[4] Q. Wang, J.-T. Wang, F. Jin, F.-D. Chi, C.-H. Zhang, Real-time dynamic hybrid testing for soil–structure interaction analysis, Soil Dynamics and Earthquake Engineering 31 (12) (2011) 1690–1702.
[5] B.M. Phillips, B.F. Spencer Jr, Model-based feedforward-feedback actuator control for real-time hybrid simulation, Journal of Structural Engineering 139 (7) (2013) 1205–1214.
[6] Y. Qian, G. Ou, A. Maghareh, S.J. Dyke, Parametric identification of a servo-hydraulic actuator for real-time hybrid simulation, Mechanical Systems and Signal Processing 48 (1–2) (2014) 260–273.
[7] G.A. Fermandois, B.F. Spencer, Model-based framework for multi-axial real-time hybrid simulation testing, Earthquake Engineering and Engineering Vibration 16 (4) (2017) 671–691.
[8] Y.-R. Dong, Z.-D. Xu, Y.-Q. Guo, Y.-S. Xu, S. Chen, Q.-Q. Li, Experimental study on viscoelastic dampers for structural seismic response control using a user-programmable hybrid simulation platform, Engineering Structures 216 (2020), 110710.
[9] X. Shao, A. Reinhorn, Development of a controller platform for force-based real-time hybrid simulation, Journal of Earthquake Engineering 16 (2) (2012) 274–295.
[10] A. Maghareh, S.J. Dyke, C.E. Silva, A self-tuning robust control system for nonlinear real-time hybrid simulation, Earthquake Engineering & Structural Dynamics 49 (7) (2020) 695–715.
[11] T. Horiuchi, T. Konno, A new method for compensating actuator delay in real–time hybrid experiments, Philosophical Transactions of the Royal Society of London. Series A: Mathematical, Physical and Engineering Sciences 359 (1786) (2001) 1893–1909.
[12] A. Darby, M. Williams, A. Blakeborough, Stability and delay compensation for real-time substructure testing, Journal of Engineering Mechanics 128 (12) (2002) 1276–1284.
[13] A. Maghareh, S.J. Dyke, A. Prakash, J.F. Rhoads, Establishing a stability switch criterion for effective implementation of real-time hybrid simulation, Smart Structures and Systems 14 (6) (2014) 1221–1245.
[14] G.A. Fermandois, Application of model-based compensation methods to real-time hybrid simulation benchmark, Mechanical Systems and Signal Processing 131 (2019) 394–416.
[15] M. Ahmadizadeh, G. Mosqueda, A. Reinhorn, Compensation of actuator delay and dynamics for real-time hybrid structural simulation, Earthquake Engineering & Structural Dynamics 37 (1) (2008) 21–42.
[16] C. Chen, J.M. Ricles, Analysis of actuator delay compensation methods for real-time testing, Engineering Structures 31 (11) (2009) 2643–2655.
[17] C. Chen, J.M. Ricles, R. Sause, R. Christenson, Experimental evaluation of an adaptive inverse compensation technique for real-time simulation of a large-scale magneto-rheological fluid damper, Smart Materials and Structures 19 (2) (2010), 025017.

[18] C. Chen, J.M. Ricles, Tracking error-based servohydraulic actuator adaptive compensation for real-time hybrid simulation, Journal of Structural Engineering 136 (4) (2010) 432–440.
[19] Y. Chae, K. Kazemibidokhti, J.M. Ricles, Adaptive time series compensator for delay compensation of servo-hydraulic actuator systems for real-time hybrid simulation, Earthquake Engineering & Structural Dynamics 42 (11) (2013) 1697–1715.
[20] P.-C. Chen, K.-C. Tsai, P.-Y. Lin, Real-time hybrid testing of a smart base isolation system, Earthquake Engineering & Structural Dynamics 43 (1) (2014) 139–158.
[21] Z. Wang, B. Wu, O.S. Bursi, G. Xu, Y. Ding, An effective online delay estimation method based on a simplified physical system model for real-time hybrid simulation, Smart Structures and Systems 14 (6) (2014) 1247–1267.
[22] P. Gawthrop, M. Wallace, S. Neild, D. Wagg, Robust real-time substructuring techniques for under-damped systems, Structural Control and Health Monitoring: The Official Journal of the International Association for Structural Control and Monitoring and of the European Association for the Control of Structures 14 (4) (2007) 591–608.
[23] R.M. Botelho, R.E. Christenson, Robust stability and performance analysis for multi-actuator real-time hybrid substructuring, in: Dynamics of Coupled Structures, Volume 4, Springer, 2015, pp. 1–7.
[24] A. Maghareh, Nonlinear robust framework for real-time hybrid simulation of structural systems: Design, implementation, and validation, Ph.D. thesis, Purdue University, 2017.
[25] S.J. Dyke, J.M. Caicedo, G. Turan, L.A. Bergman, S. Hague, Phase i benchmark control problem for seismic response of cable-stayed bridges, Journal of Structural Engineering 129 (7) (2003) 857–872.
[26] J.M. Caicedo, S.J. Dyke, S.J. Moon, L.A. Bergman, G. Turan, S. Hague, Phase ii benchmark control problem for seismic response of cable-stayed bridges, Journal of Structural Control 10 (3–4) (2003) 137–168.
[27] Y. Ohtori, R. Christenson, B. Spencer Jr, S. Dyke, Benchmark control problems for seismically excited nonlinear buildings, Journal of Engineering Mechanics 130 (4) (2004) 366–385.
[28] S. Narasimhan, S. Nagarajaiah, E.A. Johnson, H.P. Gavin, Smart base-isolated benchmark building. Part i: problem definition, Structural Control and Health Monitoring 13 (2–3) (2006) 573–588.
[29] A. Agrawal, P. Tan, S. Nagarajaiah, J. Zhang, Benchmark structural control problem for a seismically excited highway bridge—part i: Phase i problem definition, Structural Control and Health Monitoring 16 (5) (2009) 509–529.
[30] Z. Sun, B. Li, S.J. Dyke, C. Lu, L. Linderman, Benchmark problem in active structural control with wireless sensor network, Structural Control and Health Monitoring 23 (1) (2016) 20–34.
[31] C.E. Silva, D. Gomez, A. Maghareh, S.J. Dyke, B.F. Spencer Jr, Benchmark control problem for real-time hybrid simulation, Mechanical Systems and Signal Processing 135 (2020), 106381.
[32] X. Ning, Z. Wang, H. Zhou, B. Wu, Y. Ding, B. Xu, Robust actuator dynamics compensation method for real-time hybrid simulation, Mechanical Systems and Signal Processing 131 (2019) 49–70.
[33] Y. Ouyang, W. Shi, J. Shan, B.F. Spencer, Backstepping adaptive control for real-time hybrid simulation including servo-hydraulic dynamics, Mechanical Systems and Signal Processing 130 (2019) 732–754.
[34] X. Gao, S. You, Dynamical stability analysis of MDOF real-time hybrid system, Mechanical Systems and Signal Processing 133 (2019), 106261.

[35] A. Najafi, B.F. Spencer Jr, Validation of model-based real-time hybrid simulation for a lightly-damped and highly-nonlinear structural system, Journal of Applied and Computational Mechanics (2020).
[36] J. Condori, A. Maghareh, J. Orr, H.-W. Li, H. Montoya, S. Dyke, C. Gill, A. Prakash, Exploiting parallel computing to control uncertain nonlinear systems in real-time, Experimental Techniques (2020) 1–15.
[37] A. Maghareh, C.E. Silva, S.J. Dyke, Servo-hydraulic actuator in controllable canonical form: identification and experimental validation, Mechanical Systems and Signal Processing 100 (2018) 398–414.
[38] A. Maghareh, C.E. Silva, S.J. Dyke, Parametric model of servo-hydraulic actuator coupled with a nonlinear system: experimental validation, Mechanical Systems and Signal Processing 104 (2018) 663–672.
[39] J.-J.E. Slotine, W. Li, et al, Applied nonlinear control, vol. 199, Prentice hall Englewood Cliffs, NJ, 1991.
[40] R.E. Kalman, A new approach to linear filtering and prediction problems, Journal of Basic Engineering 82 (1) (1960) 35–45.
[41] MATLAB, version 9.6 (R2019a), The MathWorks Inc., Natick, Massachusetts, 2019.
[42] O. Mercan, J.M. Ricles, Stability analysis for real-time pseudodynamic and hybrid pseudodynamic testing with multiple sources of delay, Earthquake Engineering & Structural Dynamics 37 (10) (2008) 1269–1293.
[43] A. Maghareh, S.J. Dyke, A. Prakash, G.B. Bunting, Establishing a predictive performance indicator for real-time hybrid simulation, Earthquake Engineering & Structural Dynamics 43 (15) (2014) 2299–2318.
[44] A. Maghareh, S. Dyke, S. Rabieniaharatbar, A. Prakash, Predictive stability indicator: a novel approach to configuring a real-time hybrid simulation, Earthquake Engineering & Structural Dynamics 46 (1) (2017) 95–116.

Thanks for your Time